The Analysis of Parasitic Movements on a High Precision Rotation Table

D. Martin
ESRF, 6 rue Jules Horowitz, BP220, 38043 Grenoble Cedex, France

Abstract

The measurement and analysis of parasitic angle and translation movements of a high precision rotary table are presented. The table, which is used in the calibration of high precision theodolites, is capable of discriminating angular movements on its main rotation axis in the order of 0.05 arc-seconds. However, to achieve maximum performance, parasitic movements on the other 5 degrees of freedom of the table must be measured. This paper will discuss the simultaneous determination of the three translation and two tilt motions of the table using high precision capacitive probes. These probes have a range of 0.25 mm and 0.5 mm and resolution inferior to 50 nm. Both the measurement process and results are presented.

1. Introduction

For the ESRF accelerators and beamlines to work correctly, alignment is of critical importance. Alignment tolerances are typically less than one millimetre and often in the order of several micrometers. The uncertainties in the positional determination of points typically attained today at the ESRF are:

- Height determination 30 µm
- Planimetric determination 150 µm
- Tilt determination 15 µrad

The planimetric point determination is the limiting factor in the ESRF machine alignment. The semi-major axis of the absolute error ellipse, a measure of spatial quality in point determination, is aligned in the direction perpendicular to the travel of the electron beam. This radial error is in the direction most sensitive to alignment errors. It is also the direction most sensitive to angle measurements[1].

At the ESRF, all precision survey work is done with the LEICA TDA5005 motorized total station equipped with Automatic Target Recognition (ATR). For an improvement in the survey results there must be an improvement in either the distance or the angle measuring precision. At the limit of its distance measuring capacity, improvement can only be made by bettering the angle measuring uncertainty of the TDA5005. This can only be achieved by calibration [2].

2. Angle Calibration and the Theodolite Measuring Machine (TMM)

1.1. Angle Calibration Method

To improve angle measuring precision, the TDA5005 theodolite angles must be calibrated. Calibration is the act of checking or adjusting by comparison with a standard or reference the uncertainty of a measuring instrument. By definition, a standard or reference has a smaller uncertainty than the measuring instrument. The manufacturer's nominal quoted uncertainty of the TDA5005 angle encoder is 0.5 arc seconds.

The ESRF ALGE group has a very precise rotation stage coined TMM for Theodolite Measuring Machine (Figure 1). This instrument, in combination with several other instruments and techniques, is employed for the calibration of theodolite angles.

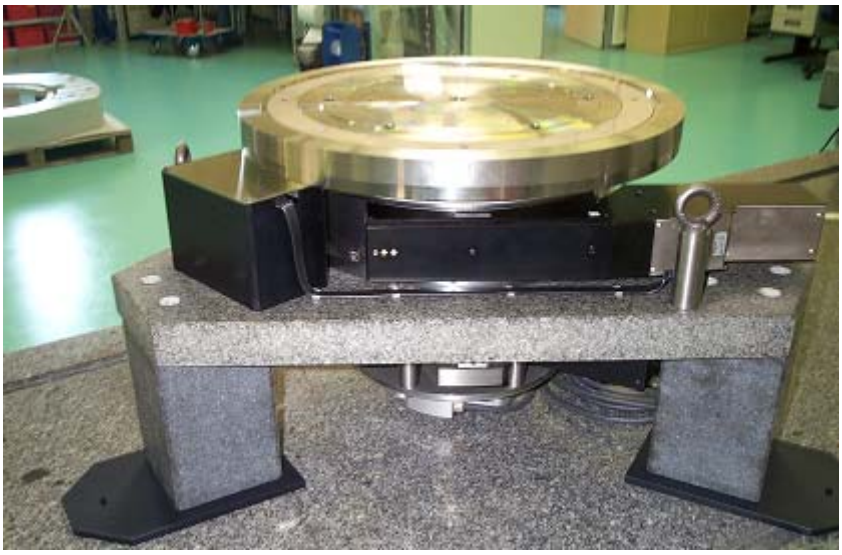

Figure 1. The ESRF ALGE Theodolite Measuring Machine (TMM).

The TMM incorporates two HEIDENHAIN RON 905 angle encoders mounted in juxtaposition to each other. One RON 905 is fixed to the main support assembly and does not move. The second RON 905 is fixed to the main plateau and rotates with it. The two RON 905 encoders are linked through a precision alignment shaft assembly. The shaft and encoders are rotated continuously by a variable speed precision rotation stage. The two RON 905 encoder positions are read out simultaneously and continuously. This configuration permits the elimination of residual encoder errors [3, 4].

To calibrate the Theodolite on the TMM; a target located at approximately 6m is sighted; the TMM is turned through an angle α; the theodolite is rotated back through the same angle; the target is re-observed; and the results compared. One of the main advantages of this method is that any angle displacement over 360° can be investigated.

1.2. Elimination of Residual Errors Using the Linked Encoders Configuration

Most systematic errors are eliminated in the RON 905 by employing four read-heads. Nevertheless, residual errors predominantly linked to the encoder interpolation system, and with incertitude of 0.36 arc seconds remain. These errors will oscillate about the true RON 905 encoder readings. This is illustrated in Figure 2. The pattern is constant and repeats itself over 360°. These errors can be largely eliminated using two angle encoders mounted in juxtaposition to each other [3, 4].

The oscillations (Figure 2) about the true angles for two RON 905 encoders for a displacement angle α are given by A_1 and A_2 in equation (1). In this equation, θ_{read} refers to the RON 905 encoder read value and θ_{true} is the true (immeasurable) angle. The subscripts *mobile* and *fixed* refer to the mobile RON 905 linked to the main plateau and the fixed RON 905 respectively. The subscript *ref* refers to the position of the encoder at an arbitrary origin angle position. It can be considered a constant.

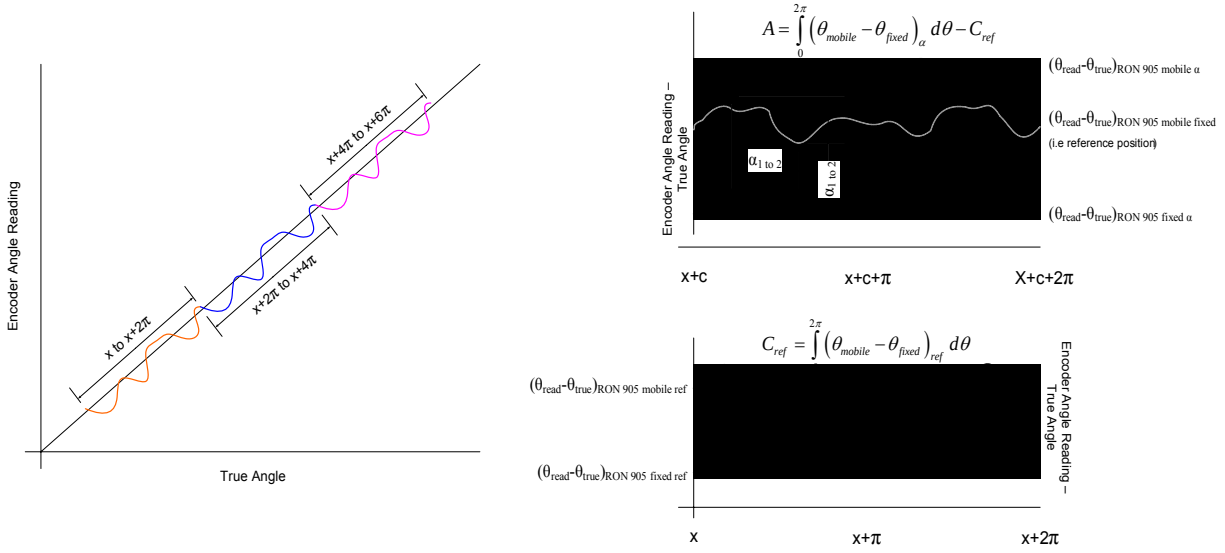

Figure 2. As the RON 905 encoder rotates about its axis, residual errors cause the angle encoder reading to oscillate about the true angle (left hand graph). These residual errors can be eliminated by employing two linked angle encoders and integrating the difference between their read values over a rotation of 2 radians (right hand graph).

In (2) the immeasurable true angles θ_{true} are eliminated by subtracting A_1 from A_2 leaving only values which are read. Dropping the *read* subscript and rearranging the equation leaves a term a_α representing the integral of the difference between the two RON 905 angle encoders over one full rotation of 2 π radians at a given angle displacement α; and a constant C_{ref} representing the integral of the difference between the two RON 905 angle encoders over one full rotation of 2 π radians at an arbitrary origin ((2) and Figure 2).

$$A_1 = \int_0^{2\pi} \left[\left(\theta_{read} - \theta_{true}\right)_\alpha - \left(\theta_{read} - \theta_{true}\right)_{ref} \right]_{mobile} d\theta$$
$$A_2 = \int_0^{2\pi} \left[\left(\theta_{read} - \theta_{true}\right)_\alpha - \left(\theta_{read} - \theta_{true}\right)_{ref} \right]_{fixed} d\theta \qquad (1)$$

$$A = A_2 - A_1$$
$$A = \int_0^{2\pi} \left[\left(\theta_{mobile} - \theta_{fixed}\right)_\alpha - \left(\theta_{mobile} - \theta_{fixed}\right)_{ref} \right] d\theta$$
$$A = \int_0^{2\pi} \left(\theta_{mobile} - \theta_{fixed}\right)_\alpha d\theta - C_{ref} \qquad (2)$$
$$A = a_\alpha - C_{ref}$$

1.3. Integral Evaluation

The problem remains of how to evaluate the integral in (2). Several possibilities exist. The first is to perform a numerical integration using the trapezoidal or some other common rule. A second possibility is to perform a curve fitting procedure on the data by approaching it as a smooth function and calculating the integral analytically.

Functional data analysis approaches discrete data with the principle that it can be represented by a smooth function which has been polluted by noise or uncertainty in the measurement process. These smooth functional observations are represented by basis functions. Polynomials, splines, wavelets and Fourier series are examples of basis functions [5].

If it is reasonably assumed that the curves $\theta_{read} - \theta_{true}$ are smooth, continuous and repeat over the interval 0 to 2 π radians; then a natural candidate for a basis function is a Fourier series. The problem with using two Fourier series to evaluate the integral described in equation (1) is the quantity of data and the form of the signal. There is a potential for several million acquisitions per second. This in and of itself requires considerable computing power to process. The form of the curve is very complex. At its base are the 36000 sinusoidal oscillations associated with the read heads. A real example is shown in Figure 3.

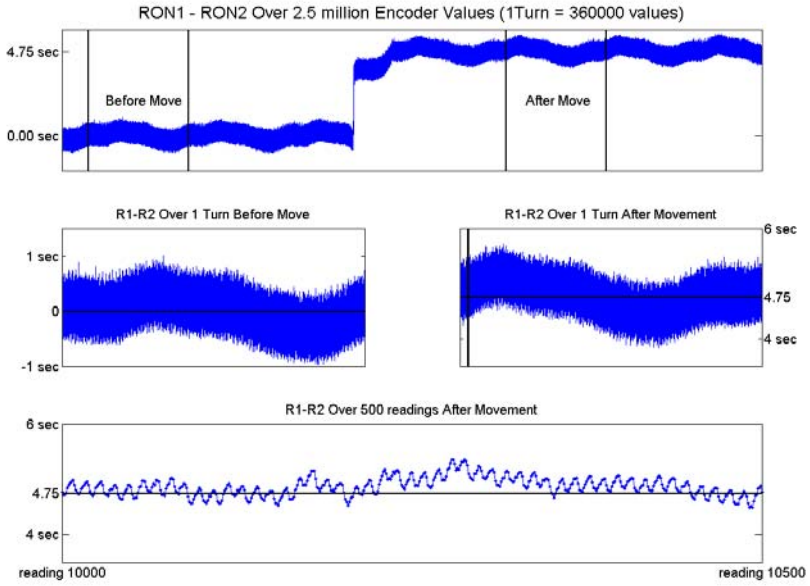

Figure 3. Real RON905 differences over a movement of 4.74 arc seconds. The top graph shows the difference between the RON 905 values over 2.5 million readings. The middle graphs show the RON905 differences over 1 turn (360000) values each while the bottom graph zooms in over reading numbers 10000 to 10500 after the movement.

Assuming that we can represent the two curves each by a Fourier series basis function, the integral of their difference, will simply be the terms $(a_0)_{curve2} - (a_0)_{curve1}$ or the mean values of the two curves. The integral of the sum of the cosine and sine terms is zero.

The ease with which the mean value is calculated makes it the best candidate for the calculation of the integral described in (1) and (2). Thus in the adopted method (equation (3)), n and m represent the number of samples taken between 0 and 2 π radians for each of the difference curves at the displacement angle α and the origin reference respectively.

$$A = \left(\frac{\sum_{i=1}^{n} (x_{mobile} - x_{fixed})_i}{n} \right)_{\alpha} - \left(\frac{\sum_{i=1}^{m} (x_{mobile} - x_{fixed})_i}{m} \right)_{ref} \qquad (3)$$

In principle, the values for θ_{fixed} and x_{fixed} in equations(1), (2) and (3) do not change. However, at each turn of the encoders, the position i is slightly different and as a result the values for θ_{fixed} and x_{fixed} will also vary slightly. The important point is that if the displacement angle α does not change the value for A in equations (2)and (3) remain constant.

1.4. Measurement Results

Angles measured by the TMM were compared to those measured by a precise autocollimator (ELCOMAT 3000) and to capacitive captor measurements. For very small angles (±30 arc seconds) the standard deviation in the difference in angles measured by the three different instruments was better than 0.03 arc seconds for a large number (2700) of angle displacements.

3. Multi-Probe Form/Spindle Error Separation

Recall the angle calibration method consists of sighting a target with the theodolite, turning the TMM through an angle, bringing the theodolite back through the same angle, re-sighting the target and comparing the results. For this to work the main theodolite and TMM axes must be coincident and all rotations of the plateau and theodolite must be identical in magnitude and opposite in sign. Clearly for very high precision work this is not the case.

For rotational movement about a principal axis as with the TMM, there will be coupled unwanted or parasitic motions associated with its other five other degrees of freedom. These error motions are: the translations along the x, y and z axes ($sx(\theta)$, $sy(\theta)$ and $sz(\theta)$); and the tilts (wobble) about the x and y axes ($w_x(\theta)$ and $w_y(\theta)$). The magnitude of these unwanted movements is dependent upon the quality of the motion stage. For the highest precision work, it is clear that the errors caused by these parasitic movements must be eliminated, minimized or compensated for.

Parasitic movements are typically measured by a probe to an artefact fixed to, or actually part of the object being moved. This probe must be independent of the object in motion. The artefact most often used is a high precision sphere. In this work the cylinder shaped TMM plateau is used. Regardless of its shape, the artefact will not be a perfect sphere or cylinder. The deviations from the sphericity or cylindricity of the artefact are referred to as form errors. In the measurement process, the parasitic spindle error motions measured by the probe are confounded with the artefact form errors. These motions must be separated from the artefact form errors.

Over the years several techniques have been developed for the accurate measure of part features. A review of many of these techniques is given in [6]. In the context of the TMM, there is essentially only one technique that can be used separate parasitic motion from form error. This is the multi-probe technique. A very clear review of this and other methods is found in [7]. These techniques are also discussed extensively in [8-14].

1.5. Radial error separation

Much of the initial work concerning the multi-probe technique is outlined in [8]. This is a model based method [6]. Model based techniques make assumptions about the form of the underlying errors. In particular, they assume the underlying error can be represented by a Fourier series.

The underlying principle of the multi-probe technique [7, 8, 11, 12] ($\geq$ three probes) is the elimination of spindle motion from the observations $m_1(\theta), m_2(\theta), m_3(\theta)\cdots$ and the subsequent recombination of the form error $f(\theta)$ by means of a Fourier series.

The general and experimental setup for the multi-probe technique is shown in Figure 4. The probes themselves are positioned at angles $\varphi_2, \varphi_3\cdots$ with respect to probe no. 1 which is aligned along the x axis (i.e. $\varphi_1 = 0$). Measurements from the different probes $m_1(\theta), m_2(\theta), m_3(\theta)\cdots$ are made simultaneously.

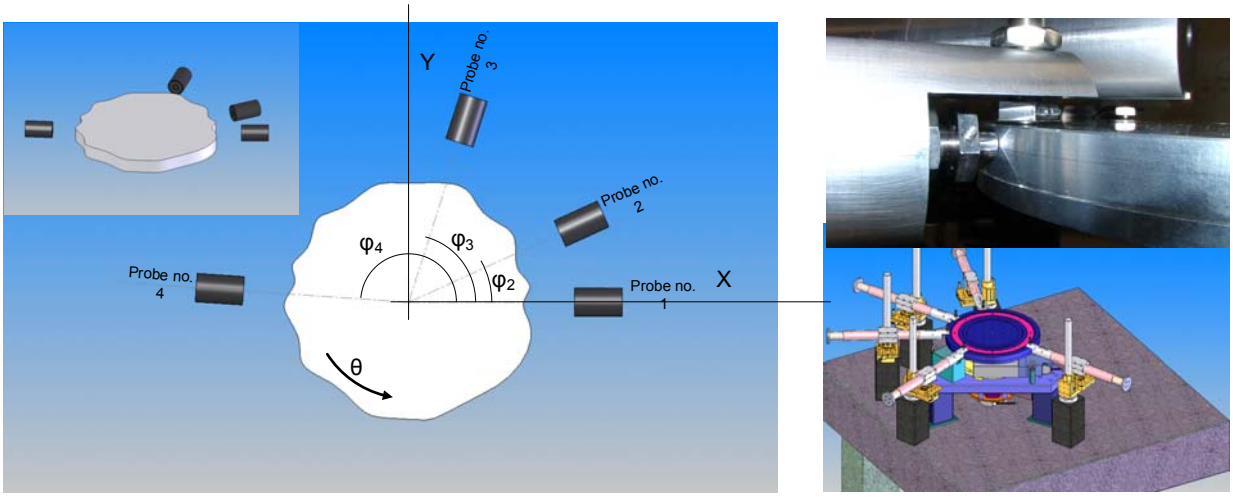

Figure 4 Setup for the multi-probe method of motion/form error separation. Several probes are arranged around the artefact at angles $\varphi_2, \varphi_3 \cdots$. We take probe no. 1 to be aligned along the x axis. The probes are stationary and make readings $m_1(\theta), m_2(\theta), m_3(\theta) \cdots$ while the artefact rotates about its z axis. The right hand side of the graph shows a photograph of the capacitive probe setup and a drawing of the experimental setup used in the tests described below.

The probe readings can be represented by equation (4). Here $sx(\theta)$ and $sy(\theta)$ are x and y spindle error motions. There are n probes in the setup.

$$\begin{aligned} m_1(\theta) &= f(\theta) + sx(\theta) \\ m_2(\theta) &= f(\theta - \varphi_2) + sx(\theta)\cos(\varphi_2) + sy(\theta)\sin(\varphi_2) \\ &\vdots \\ m_n(\theta) &= f(\theta - \varphi_n) + sx(\theta)\cos(\varphi_n) + sy(\theta)\sin(\varphi_n) \end{aligned} \tag{4}$$

A new function $M(\theta)$ can be created by multiplying the measurement equations $m(\theta)_i \rightarrow i = 1 \cdots n$ in (4) by weighting coefficients $1, a_2 \cdots a_n$ and summing the results (equations (5) and (6)).

$$M(\theta) = m_1(\theta) + a_2 m_2(\theta) + \cdots + a_n m_n(\theta) \tag{5}$$

$$\begin{aligned} M(\theta) &= f(\theta) + sx(\theta) + a_2\left(f(\theta - \varphi_2) + sx(\theta)\cos(\varphi_2) + sy(\theta)\sin(\varphi_2)\right) + \cdots \\ &\quad \cdots + a_n\left(f(\theta - \varphi_n) + sx(\theta)\cos(\varphi_n) + sy(\theta)\sin(\varphi_n)\right) \\ &= f(\theta)(1 + a_2 + \cdots + a_n) \\ &\quad + sx(\theta)\left(1 + a_2\cos(\varphi_2) + \cdots + a_n\cos(\varphi_n)\right) \\ &\quad + sy(\theta)\left(a_2\sin(\varphi_2) + \cdots + a_n\sin(\varphi_n)\right) \end{aligned} \tag{6}$$

Imposing the condition (7) eliminates the spindle error contributions $sx(\theta)$ and $sy(\theta)$ by forcing them to be zero. The weighting factors $a_i \rightarrow i = 2 \cdots n$ are found by solving the simultaneous set of equations (7).

$$\begin{aligned} a_2\cos(\varphi_2)+a_3\cos(\varphi_3)+\cdots+a_n\cos(\varphi_n)+1=0 \\ a_2\sin(\varphi_2)+a_3\sin(\varphi_3)+\cdots+a_n\sin(\varphi_n)+0=0 \end{aligned} \tag{7}$$

In equation (7), there are two equations for n unknown constants. Therefore a minimum of two coefficients a_2 and a_3 (i.e. three probes) are required to satisfy (7). In the three-probe form error spindle motion separation technique, the weighting coefficients are defined by the orientation angles φ_2 and φ_3 of the probes and are given by $a_2=\sin\varphi_3/\sin(\varphi_2-\varphi_3)$ and $a_3=-\sin\varphi_2/\sin(\varphi_2-\varphi_3)$. More probes give $n-3$ degrees of freedom in selecting $(a_3\cdots a_n)$ and theoretically avoid harmonic suppression and improve measurement accuracy. Other problems, most notably their alignment can reduce the advantages of more than 3 probes. Several propositions for the selection of the weighting coefficients $(a_3\cdots a_n)$ when more than three probes are used are discussed in [15].

It is assumed that the form error $f(\theta)$ can be represented by a Fourier series where A_k and B_k are the Fourier coefficients

$$f(\theta)=\sum_{k=1}^{\infty}\left(A_k\cos k\theta+B_k\sin k\theta\right) \tag{8}$$

Substituting (8) into the summed result of equation (6), expanding, then using angle addition identities and collecting common terms of $A_k\cos k\theta$, $A_k\sin k\theta$, $B_k\cos k\theta$ and $B_k\sin k\theta$ gives (9).

$$\begin{aligned} M(\theta) \;=\; & \sum_{k=1}^{\infty}A_k\cos k\theta\left(1+a_2\cos k\varphi_2+\cdots a_n\cos k\varphi_n\right) \;\cdots \\ & +\sum_{k=1}^{\infty}A_k\sin k\theta\left(a_2\sin k\varphi_2+\cdots a_n\sin k\varphi_n\right) \;\cdots \\ & +\sum_{k=1}^{\infty}B_k\sin k\theta\left(1+a_2\cos k\varphi_2+\cdots a_n\cos k\varphi_n\right) \;\cdots \\ & +\sum_{k=1}^{\infty}B_k\cos k\theta\left(a_2\sin k\varphi_2+\cdots a_n\sin k\varphi_n\right) \end{aligned} \tag{9}$$

Defining the terms $\alpha_k=1+a_2\cos k\varphi_2+\cdots a_n\cos k\varphi_n$ and $\beta_k=a_2\sin k\varphi_2+\cdots a_n\sin k\varphi_n$; and remarking from equation (7) that when $k=1$, both $\alpha_1=0$ and $\beta_1=0$ gives equation(10).

$$M(\theta)=\sum_{k=2}^{\infty}\left(A_k\alpha_k-B_k\beta_k\right)\cos k\theta+\sum_{k=2}^{\infty}\left(A_k\beta_k+B_k\alpha_k\right)\sin k\theta \tag{10}$$

Coefficients F_k and G_k in (11), are found by calculating the discrete Fourier series of the summed probe readings $M(\theta)$ in (5), and the coefficients A_k and B_k of (8) are found by solving the matrix equation (12).

$$M(\theta)=\sum_{k=2}^{m}\left(F_k\cos k\theta+G_k\sin k\theta\right) \tag{11}$$

$$\begin{pmatrix}\alpha_k & -\beta_k\\ \beta_k & \alpha_k\end{pmatrix}\begin{pmatrix}A_k\\ B_k\end{pmatrix}=\begin{pmatrix}F_k\\ G_k\end{pmatrix}$$

$$A_k=\frac{F_k\alpha_k+G_k\beta_k}{\alpha_k^2+\beta_k^2} \tag{12}$$

$$B_k=\frac{F_k\beta_k-G_k\alpha_k}{\alpha_k^2+\beta_k^2}$$

In equations (11) and (12) $k=2\cdots m$, where m is the number of discrete harmonics used in the Fourier series. The $k=1$ harmonic represents the eccentricity or centring error of the principal axis of the

artefact and the rotation stage. This once around error is generally removed from radial motion error measurements [7]. It contains no $f(\theta)$, $sx(\theta)$ or $sy(\theta)$ information.

With A_k and B_k determined, $f(\theta)$ is calculated from (8), and finally $sx(\theta)$ and $sy(\theta)$ are derived from (4).

$$sx(\theta) = m_1(\theta) - f(\theta) \quad sy(\theta) = \left(m_2(\theta) - f(\theta) - sx(\theta)\cos\varphi_2\right) / \sin\varphi_2$$

1.6. Face error separation

The multi-probe error separation can also be used to determine the axial $sz(\theta)$ and wobble $w_x(\theta)$ and $w_y(\theta)$ error motions by separating them from the artefact vertical face form error $f(\theta)$. The equations for the n probe readings are given by equation(13).

$$\begin{aligned} m_1(\theta) &= f(\theta) + sz(\theta) + w_x(\theta) \\ m_2(\theta) &= f(\theta - \varphi_2) + sz(\theta) + w_x(\theta)\cos(\varphi_2) + w_y(\theta)\sin(\varphi_2) \\ &\vdots \\ m_n(\theta) &= f(\theta - \varphi_n) + sz(\theta) + w_x(\theta)\cos(\varphi_n) + w_y(\theta)\sin(\varphi_n) \end{aligned} \tag{13}$$

With four unknowns in (13), a minimum of four probes are required. As with the multi-probe radial separation technique the measurement equations $m(\theta)_i \rightarrow i = 1 \cdots n$ in (13) are multiplied by weighting coefficients $1, a_2 \cdots a_n$ and the results summed eliminating axial $sz(\theta)$ and wobble $w_x(\theta)$ and $w_y(\theta)$ error motions contributions analogous to (6).

The coefficients $a_2 \cdots a_n$ are found in the same way as (7). With four probes the coefficients are a_2, a_3 and a_4 are fixed. More probes give $n-4$ degrees of freedom in selecting $a_5 \cdots a_n$ and can theoretically avoid harmonic suppression and improve measurement accuracy [13, 15]. Once again this improvement is strongly dependent upon probe alignment.

The solution to the form error follows analogously the radial error separation technique described in equations (8) to (12). With the $f(\theta)$ known, $sz(\theta)$, $w_x(\theta)$ and $w_y(\theta)$ can be determined by solving (14) by least squares.

$$\begin{pmatrix} 1 & 1 & 0 \\ 1 & \cos(\varphi_2) & \sin(\varphi_2) \\ & \vdots & \\ 1 & \cos(\varphi_n) & \sin(\varphi_n) \end{pmatrix} \begin{pmatrix} sz(\theta) \\ w_x(\theta) \\ w_y(\theta) \end{pmatrix} = \begin{pmatrix} m(\theta)_1 - f(\theta) \\ m(\theta)_2 - f(\theta - \varphi_2) \\ \vdots \\ m(\theta)_n - f(\theta - \varphi_n) \end{pmatrix} \tag{14}$$

1.7. Measurement Results

This section examines the three-probe radial and four point face form error spindle motion separation technique using redundant measurements. Five probe supports were installed around the TMM plateau as shown in Figure 4. Two probes, one measuring horizontal displacement and the other vertical displacement were installed on each probe support. The horizontal probes had a nominal range of 250μm while the vertical probes had a range of 500 μm.

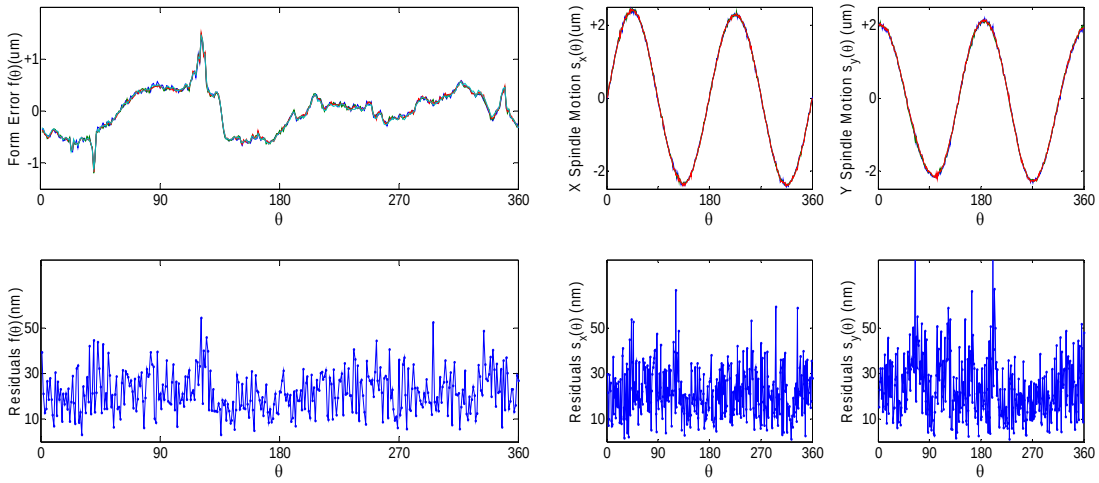

Figure 5 Results of radial form error spindle motion separation. The top left graph shows the horizontal artefact form error. The top middle and right graphs show the x and y spindle motions respectively. The bottom graphs show the residual errors of the 6 measurement series used in the test. The residual standard deviations are better than 25 nm.

There are 10 possible three probe combinations of the five radial probe measurements. The overall standard deviation for the 10 measurement series was 31 nm. Of the 10 radial combinations, four were found to be relatively noisy. This is certainly due to probe alignment which is a problematic with this technique. Removing the four problematic measurement series results in an overall standard deviation of 23 nm for the form error and x and y spindle motion determinations. These results are shown in Figure 5.

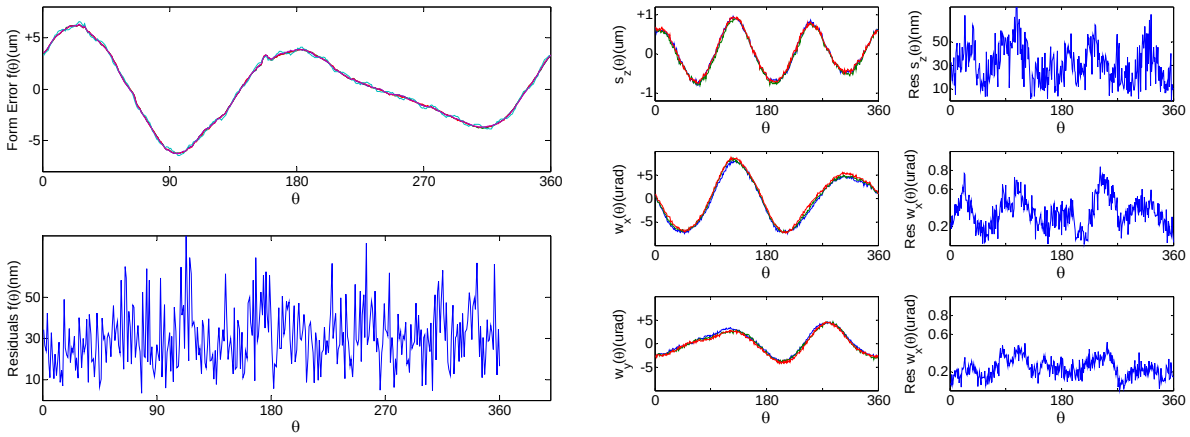

Figure 6 Results of face form error spindle motion separation. The top left graph shows the vertical artefact form error. The bottom left graph shows the residuals with respect to the mean of the four good data series for the form error. The mean residual standard deviation is 31 nm. The three middle graphs show the sz , w_x and w_y spindle motions respectively. The three right hand graphs show the residual errors of the spindle motions of the four good series with respect to their mean curves. The residual standard deviations are 31 nm, 0.35 µrad and 0.24 µrad respectively.

There are five possible four probe combinations for the five face probe measurements. The overall mean standard deviation for the form error determination of the five combinations is 79 nm. Of the five combinations, one was found to be particularly noisy. Removing this series gives an overall mean

standard deviation in the face form error determination of 31 nm. The uncertainties in $sz(\theta)$, $w_x(\theta)$ and $w_y(\theta)$ once again ignoring the noisy data series are 31 nm, 0.35 µrad and 0.24 µrad respectively. Results for these comparative tests are shown in Figure 6.

4. Conclusions

The TMM, which is used in the calibration of high precision theodolites, is capable of discriminating angular movements on its main rotation axis better than 0.05 arc-seconds. However, to achieve maximum performance, parasitic movements on the other 5 degrees of freedom of the table must be measured. It has been shown that it is possible to make a simultaneous determination of the three translation and two tilt motions of the table using high precision capacitive probes. The uncertainties in the parasitic error motion determination are less than 50 nm and 0.5 µrad for translational and rotational movements respectively.

5. References

1. Martin, D. *Instrumentation and Survey Networks at the ESRF*. in *Eigth International Workshop on Accelerator Alignment*. 2004. CERN, Geneva Switzerland.
2. Martin, D. *Instrumentation and Calibration at the ESRF*. in *Seventh International Workshop on Accelerator Alignment*. 2002. SPRING-8, Japan.
3. Leleu, S., *Contribution a l'Evaluation de Angles - Conception, Realisation et Validation dún Plateau Pivotant de Tres Haute Precision : Vers une Nouvelle Reference Angulaire Nationale*, in *Mevanique*. 2000, Ecale Nationale Supérieure dÁrts et Métiers: Metz. p. 233.
4. Palmer, E.W., *Goniometer with Continuously Rotating Gratings for Use as an Angle Standard.* Precision Engineering-Journal of the American Society for Precision Engineering, 1988. **10**(3): p. 147-152.
5. Ramsay, J.O. and B.W. Silverman, *Functional data analysis*. Springer series in statistics. 1997, New York ; London: Springer. xiv, 310.
6. Evans, C.J., R.J. Hocken, and W.T. Estler, *Self Calibration: Reversal, Redundancy, Error Separation, and 'Absolute Testing'.* Annals of the CIRP, 1996. **45**(2): p. 617-633.
7. Grejda, R.D., *Use and Calibration of Ultraprecision Axes of Rotation With Nanometer Level Metrology*, in *Mechanical Engineering*. 2002, The Pennsylvania State University. p. 135.
8. Whitehouse, D.J., *Some Theoretical Aspects of Error Separation Techniques in Surface Metrology.* Journal of Physics E-Scientific Instruments, 1976. **9**(7): p. 531-536.
9. Chetwynd, D.G. and G.J. Siddall, *Improving the Accuracy of Roundeness Measurement.* Journal of Physics E-Scientific Instruments, 1976. **9**(7): p. 537-544.
10. Moore, D., *Design Considerations in Multiprobe Roundness Measurement.* Journal of Physics E-Scientific Instruments, 1989. **22**(6): p. 339-343.
11. Zhang G.X. and Wang R.K., *Four-Point Method of Roundness and Spindle Error Motion Measurements.* CIRP, 1993. **42**(1): p. 593-596.
12. Zhang G.X., et al., *A Multi-Point Method for Spindle Error Motion Measurement.* CIRP, 1997. **42**(1): p. 441-445.
13. Zhang, G.X. and R.K. Wang, *Four-point method of roundness and spindle error motion measurement.* CIRP, 1993. **42**(1): p. 593-596.
14. Marsh E., Couey J., and Vallance R., *Nanometer–Level Comparison of Three Spindle Error Motion Separation Techniques.* http://mdrl.mne.psu.edu/spindle.htm, 2005.
15. Zhang, G.X., et al., *A multipoint method for spindle error motion measurement.* CIRP, 1997. **46**(1): p. 441-445.